Spectral complex conductivity inversion of airborne electromagnetic data

Jonathan W. Goold, Leif H. Cox, and Michael S. Zhdanov, University of Utah*

SUMMARY

The spectral induced polarization (IP) method is a powerful tool for mineral exploration. However, until recently, this method was applied as a ground based geophysical survey method only. In this paper, we examine the possibility of inverting for spectral resistivity in frequency domain airborne electromagnetic data. Our study is based both on forward modeling and inversion of synthetic electromagnetic data for models with complex frequency-dependent conductivity. Numerical modeling study and field data inversion demonstrate the possibility of developing an airborne version of the spectral IP method.

INTRODUCTION

Electromagnetic (EM) data observed in geophysical experiments, in general, reflect two phenomena: 1) electromagnetic induction (EMI) in the earth, and 2) an induced polarization (IP) effect related to the relaxation of polarized charges in rock formations (Zonge and Wynn, 1975). The IP effect is caused by complicated physical-chemical polarization processes that accompanies current flow in the earth. It is manifested the by frequency-dependent complex resistivity of exploration targets. This effect is taken into account in the spectral IP method, which is a powerful technique for mineral exploration.

Typically, the spectral IP method is applied as a ground geophysical survey only. The spectral IP effect is not taken into account in the interpretation of airborne electromagnetic (AEM) data, especially in the case of three-dimensional (3D) inversion. Recently, CEMI has developed a new version of the inversion software for interpretation of frequency domain AEM data. This software is based on the localized quasi-linear (LQL) approximation followed by rigorous inversion. In particular, this software allows us to invert for complex conductivity using the LQL approximation.

In this paper, we use this new software to examine the possibility of inverting for spectral resistivity in HEM data. Our study is based on forward modeling and inversion of synthetic EM data for the models with complex frequency-dependent conductivity. We also apply this technique to field data and compare the inverted spectral complex conductivity to ground based IP interpretation and known geology.

COLE-COLE CONDUCTIVITY RELAXATION MODELS

It is well understood that the effective conductivity of rocks is not necessarily a constant and real number, but may vary with frequency and be complex. There are several physical explanations for effective conductivity. Most often they are explained by the physical-chemical polarization effects of the mineralized particles of the rock material, and/or by electrokinetic effects in the pores of a reservoir (Wait, 1959; Luo and Zhang, 1998).

It was demonstrated in the pioneer work of Pelton (1977) that the Cole-Cole relaxation model (Cole and Cole, 1941) well represents the typical complex conductivity of polarized rock formations. In the framework of this model, the complex resistivity, $\rho(\omega)$, is described by the following well-known expression:

$$\rho(\omega) = \rho\left(1 - \eta\left(1 - \frac{1}{1 + (i\omega\tau)^{C}}\right)\right), \tag{1}$$

where ρ is the DC resistivity (Ohm-m); ω is the angular frequency (rad/sec), τ is the time parameter; η is the intrinsic chargeability (Seigel, 1959), and C is the relaxation parameter. The dimensionless intrinsic chargeability, η, characterizes the intensity of the IP effect.

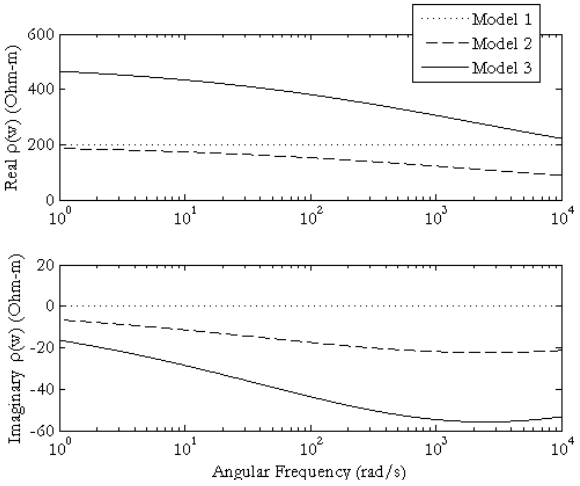

Figure 1: Cole-Cole predicted behavior of complex resistivity for three synthetic models. The upper panel presents the real part of the complex resistivity, while the bottom panel presents the imaginary part.

Figure 1 presents examples of typical complex resistivity curves with the Cole-Cole model parameters defined according by Table 1.

Table 1: Cole-Cole parameters for synthetic models.

Model 1	Model 2	Model 3
$\rho_1 = 200(\Omega - m)$	$\rho_2 = 200\ (\Omega - m)$	$\rho_3 = 500(\Omega - m)$
$\eta_1 = NA$	$\eta_2 = 0.911$	$\eta_3 = 0.911$
$\tau_1 = NA$	$\tau_2 = 6.3x10^{-5}$	$\tau_3 = 6.3x10^{-5}$
$C_1 = NA$	$C_2 = 0.306$	$C_3 = 0.306$

One can see the significant difference between the dotted, dashed and solid curves in this plot, which correspond to the different synthetic models with different Cole-Cole parameters.

Note also that the Cole-Cole curve gives us just one possible example of a relaxation model. There are several other models discussed in geophysical literature (Pelton, 1977; Zhdanov, 2006, e.g.). However, in this paper we will restrict our study to the models with the complex resistivity described by the Cole-Cole expression (1).

BACKGROUND OF THE LQL INVERSION

For completeness, we begin our paper with a short review of the basic principles of LQL inversion. This approximation is based on the quasi-linear approximation (Zhdanov and Fang, 1996b), which assumes that the anomalous field, $\mathbf{E}^a$, inside the inhomogeneous domain is linearly proportional to the background field, $\mathbf{E}^b$, through some reflectivity tensor, $\widehat{\lambda}$. In the current LQL formulation, we also make the assumption that the reflectivity tensor is a scaler and is source independent:

$$\mathbf{E}_I^a(\mathbf{r}) \approx \lambda(\mathbf{r}) \cdot \mathbf{E}_I^b(\mathbf{r}), \tag{2}$$

where $\mathbf{r} = (\mathbf{x}, \mathbf{y}, \mathbf{z})$ is a point inside the inversion domain and I indicates the transmitter number.

Substituting formula (2) into the corresponding integral equation for the anomalous electric field, we obtain integral representations for the LQL approximation of the anomalous magnetic field:

$$\mathbf{H}^a_{LQL}(\mathbf{r}_j) = \mathbf{G}_H\left(\Delta\sigma(\mathbf{I}+\lambda(\mathbf{r}))\cdot\mathbf{E}^b(\mathbf{r})\right) \approx \mathbf{G}_H[\Delta\sigma\cdot\mathbf{E}], \quad (3)$$

where $\mathbf{I}$ is the identity tensor, $\mathbf{r}_j$ is the observation point and $\mathbf{G}_E$ and $\mathbf{G}_H$ are the corresponding Green's linear operators.

Following Zhdanov and Fang (1996a) and Zhdanov and Tartaras (2002), we introduce a new tensor function:

$$m(\mathbf{r}) = \Delta\sigma(\mathbf{r})(1+\lambda(\mathbf{r})), \quad (4)$$

which we call a modified material property parameter.

Equation (3) takes the form:

$$\mathbf{H}^a_{LQL}(\mathbf{r}_j) = \mathbf{G}_H\left(m(\mathbf{r})\mathbf{E}^b(\mathbf{r})\right), \quad (5)$$

which is linear with respect to the material property function $m(\mathbf{r})$. We can solve the linear equation, (5) with respect to $m(\mathbf{r})$, which is source independent. Now, a scalar reflectivity coefficient, $\lambda(\mathbf{r})$, is determined, based on the condition:

$$\|\lambda(\mathbf{r})\mathbf{I} - \mathbf{G}_E(m(\mathbf{r}))\|_{L_2(D)} = \min. \quad (6)$$

Knowing $\lambda(\mathbf{r})$ and $m(\mathbf{r})$, we can find $\Delta\sigma(\mathbf{r})$ from equation (4).

We can use the LQL approximation 3D inversion of both electromagnetic induction and induced polarization effects in inhomogeneous structures. In order to take into account the IP effect, the expression for the anomalous conductivity, $\Delta\sigma$, should be substituted now by another, complex value, $\Delta\widetilde{\sigma}$, which may be described by the relaxation Cole-Cole model (equation 1):

$$\Delta\widetilde{\sigma} = \sigma\left(1-\eta\left(1-\frac{1}{1+(i\omega\tau)^C}\right)\right)^{-1} - \sigma_b. \quad (7)$$

INVERSION OF THE SYNTHETIC AEM DATA

Synthetic frequency-domain AEM data has been generated using computer code INTEM3DIP for three geoelectrical models (Figures 2 and 3). EM data are synthesized over nine different horizontal coplanar channels: 10, 50, 100, 500, 1000, 1760, 5000, 7040 and 10,000 Hz. Five flight lines 180 m long spaced 25 m apart with a data sample recorded every 30 m along the flight line are simulated.

A simple geoelectrical block model is centered beneath each synthetic survey. The models consist of an anomalous domain that is a 50 m cube located 50 m beneath the surface. The cube is discretized into thirty-two 12.5 x 12.5 x 25 m^3 blocks. The homogeneous background conductivity for the models is 2 mS/m. The Cole-Cole parameters of the resistivity relaxation curves for these models are shown in Table 1.

Model 1 has a total resistivity in the anomalous block of 5 mS/m. This value is purely real, with no imaginary resistivity present in this model.

The conductivity in Model 2 has both anomalous real and imaginary parts, given by the Cole-Cole parameters in Table 1. The intrinsic chargeability and relaxation parameter for this model are taken from empirical measurements of a massive sulfide deposit by Pelton et al.

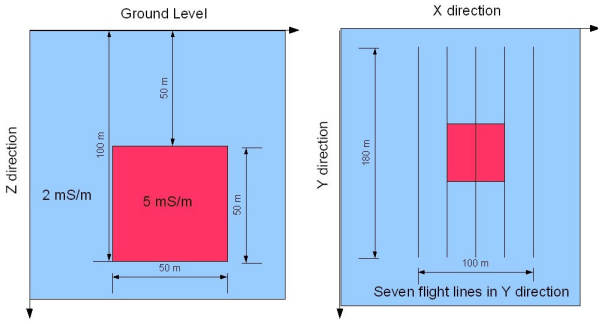

Figure 2: Vertical slice and plane view of geoelectrical model and survey configuration for Model 1 and Model 2.

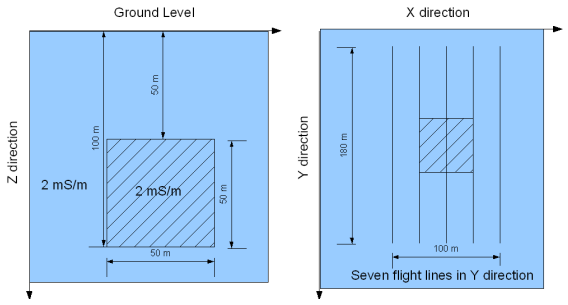

Figure 3: Vertical slice and plane view of geoelectrical model and survey configuration for Model 3.

(1978). These values were selected for the synthetic models because of the relatively high value of the relaxation parameter. The high relaxation of the Cole-Cole model will maximize the peak of the imaginary conductivity anomaly. The time constant is taken from empirical measurements of magnetite, also by Pelton. Note that the lower the time constant, the higher the frequency range for the imaginary response. A time constant in the range of 1e-2 to 1e-4 generally produces a peak response in the imaginary conductivity within the bandwidth of current FD AEM technology. The empirical measurements collected by Pelton et al. (1978) suggest that many different ore deposit types have a peak IP response within this bandwidth.

Model 3 has a total DC conductivity equal to background, but at the frequency ranges synthesized, it has both real and imaginary anomalous conductivities. The Cole-Cole parameters causing this response are the same as in Model 2.

We inverted the synthetic AEM data in an attempt to recover the complex conductivities using the CEMI code FD_AEMInv_C. The inversion domain is discretized into 6,144 cells of size 12.5 x 12.5 x 12.5 m^3. The entire inversion domain is 200 x 200 x 300 m^3. Inversion over each of the nine frequencies was carried out individually for each synthetic model. The misfit cutoff for each inversion was set below 3 percent.

The results of the inversion for the model with constant conductivity, Model 1, produce approximately constant values for the inverted real and imaginary conductivity within the entire frequency range (Figure 4). The real part of the inverted conductivity is close to the true conductivity of the model, 5 mS/m. The imaginary part of the inverted conductivity is essentially zero. This result demonstrates that our inversion does not generate an artificial imaginary conductivity for this synthetic model which has no IP effect.

The results of the inversion for Models 2 and 3, the models with Cole-

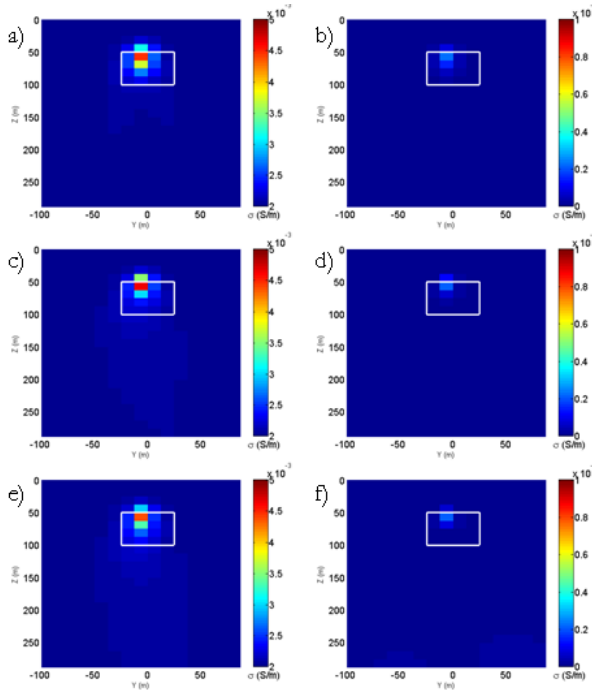

Figure 4: Vertical sections of the conductivity distribution obtained by LQL inversion of the synthetic airborne data for Model 1: a) real conductivity at a frequency of 10 Hz, b) 10 Hz imaginary conductivity, c) 100 Hz real conductivity, d) 100 Hz imaginary conductivity, e) 1 kHz real conductivity, f) 1 kHz imaginary conductivity.

Cole parameters governing the anomalous conductivity, show an increase in the real and imaginary conductivity within the anomalous domain as the frequency increases. (See, for example, the inversion results for Model 3 in Figure 5.) This increase corresponds well with the behavior of the Cole-Cole parameters of the true models. The maximum complex conductivity from the inversion has been selected and plotted against frequency in Figure 6.

The results of our modeling study indicate complex conductivity distribution can be recovered, in principle, from observed AEM data.

INVERSION OF FIELD AEM DATA

We test this spectral complex method on field data from a DIGHEM survey. For this study, we have selected a 1.6 km^2 subset of the airborne data with a known geologic target. The target area contains a shear zone, with a thin conductive graphitic shale on the footwall and a mineralized resistive body on the hanging wall. The target zone exhibits an IP response, as interpreted from a ground based gradient array survey.

Two different joint inversions were performed using the methods described above, one using the 872 Hz coplanar and 1029 Hz coaxial, which we term the low frequency inversion, and the other using the 5536 Hz coaxial and 7189 Hz coplanar channels, referred to as the high frequency inversion. The inversion domain is discretized into 151,200 cells of size 15 x 15 x 15 m^3, with 344 soundings used per channel.

A two dimensional slices of the 3D inversion results are plotted across geologic strike in Figure 7. A red line is inserted at the approximate location of the boundary between the shale and resistor. This location is taken from drilling and time domain EM interpretation, and the dip

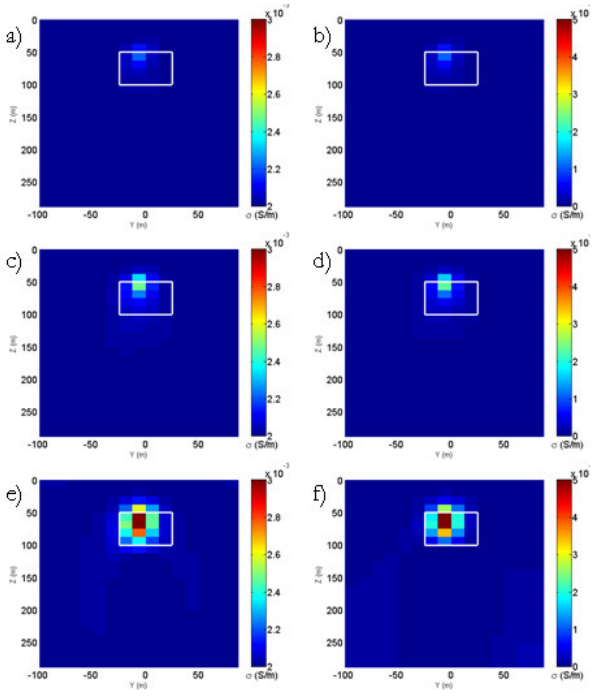

Figure 5: Vertical sections of the conductivity distribution obtained by LQL inversion of the synthetic airborne data for Model 3: a) real conductivity at a frequency of 10 Hz, b) 10 Hz imaginary conductivity, c) 100 Hz real conductivity, d) 100 Hz imaginary conductivity, e) 1 kHz real conductivity, f) 1 kHz imaginary conductivity.

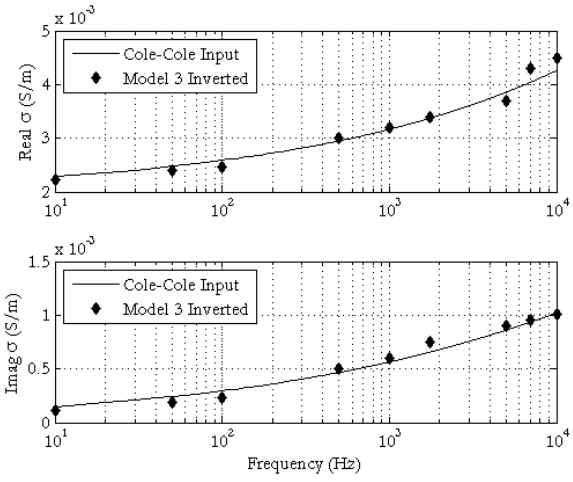

Figure 6: Model 3 inversion results (diamonds) with the true frequency dependent conductivity (solid lines).

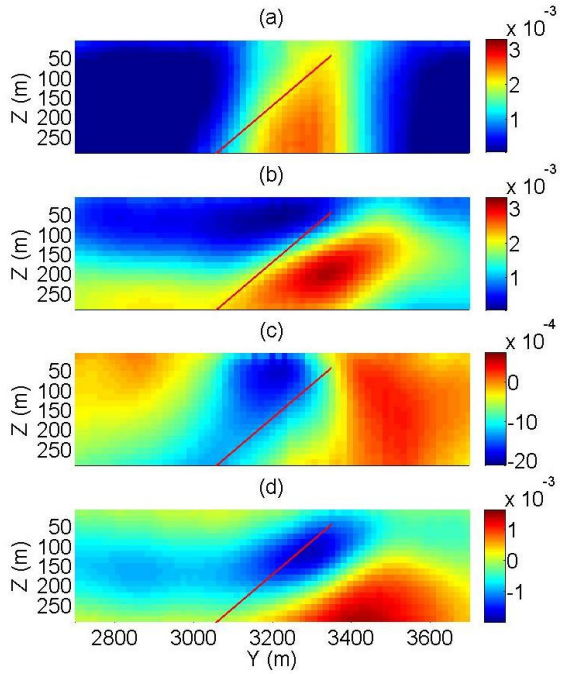

Figure 7: Inversion results for DIGHEM field data set. The colorbar units are S/m. The plots are as follows: a) real conductivity of joint inversion of low frequency channels, b) real conductivity of joint inversion of high frequency channels, c) imaginary conductivity of joint inversion of low frequency channels, and d) imaginary conductivity of joint inversion of high frequency channels.

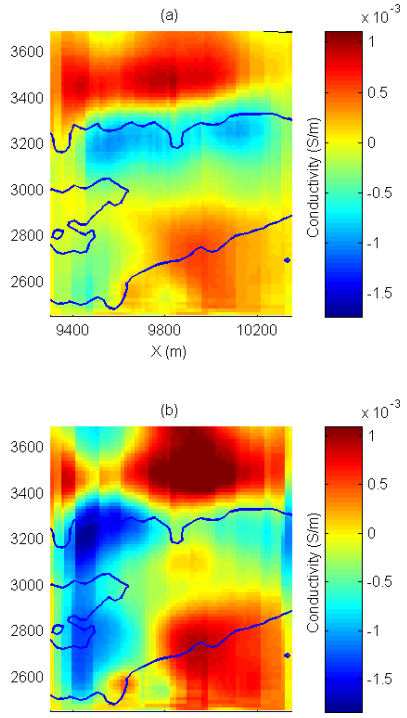

Figure 8: Imaginary part of the complex conductivity inversion with gradient array interpreted chargeability overlaid. The chargeability contour is at 22 ms. The inversion results from both the low frequency channel (a) and the high frequency channel (b) show good spatial correlation with the ground based chargeability.

is confirmed by local geology outcrops. The top of the line represents the top of the shale.

We interpret the conductivity high in the real part of the complex conductivity to indicate the location of the conductive shale. The depth to top and dip of the conductor are resolved in the real part of the conductivity. The large negative in the imaginary conductivities also demonstrates the local geologic dip. This feature is offset towards the hanging wall of the fault and slightly above the large real conductivity high. This location corresponds to the resistive mineralized zone. The large negative also correlates well with the ground based gradient array interpretation, as shown in Figure 8.

The spectral complex conductivity inversion of the airborne data corresponds well to the known target geometry. The complex part of the conductivity clearly correlates with the ground based gradient array chargeability interpretation. We also see an increase in the real conductivity with frequency, as would be expected from any model using the Cole-Cole curve.

CONCLUSION

Synthetic forward modeling and inversion exercises suggest the recovery of Cole-Cole model parameters from FD AEM data may be possible. The frequency range of FD AEM data systems correspond well with many of the peak imaginary conductivity anomalies identified by Pelton et al. (1978). In addition, the correlation of the field data inversion results to the ground based IP interpretation is encouraging. This research shows that inversion for spectral complex conductivity may add additional information to airborne EM data interpretation. More research needs to be done before the airborne spectral IP method may become a practical tool for mineral exploration.

ACKNOWLEDGMENTS

The authors acknowledge the support of the University of Utah Consortium for Electromagnetic Modeling and Inversion (CEMI), which includes BAE Systems, Baker Atlas Logging Services, BGP China National Petroleum Corporation, BHP Billiton World Exploration Inc., British Petroleum, Centre for Integrated Petroleum Research, EMGS, ENI S.p.A., ExxonMobil Upstream Research Company, INCO Exploration, Information Systems Laboratories, MTEM, Newmont Mining Co., Norsk Hydro, OHM, Petrobras, Rio Tinto - Kennecott, Rocksource, Russian Research Center Kurchatov Institute, Schlumberger, Shell International Exploration and Production Inc., Statoil, Sumitomo Metal Mining Co., and Zonge Engineering and Research Organization.

We are thankful to Dr. Perry Eaton and Jeremy Cook of Newmont Mining Company for providing the field data and permission to publish the results.